INTERFACE

royalsocietypublishing.org/journal/rsif

Research

Cite this article: Gawthrop PJ, Pan M. 2022 Energy-based advection modelling using bond graphs. *J. R. Soc. Interface* **19**: 20220492. https://doi.org/10.1098/rsif.2022.0492

Received: 7 July 2022
Accepted: 21 September 2022

Subject Category:
Life Sciences–Engineering interface

Subject Areas:
bioenergetics, systems biology, computational biology

Keywords:
systems biology, advection, physiome, bond graph

Author for correspondence:
Peter J. Gawthrop
e-mail: peter.gawthrop@unimelb.edu.au

THE ROYAL SOCIETY PUBLISHING

Energy-based advection modelling using bond graphs

Peter J. Gawthrop[1] and Michael Pan[1,2]

[1]Systems Biology Laboratory, School of Mathematics and Statistics, and Department of Biomedical Engineering, and [2]School of Mathematics and Statistics, Faculty of Science, University of Melbourne, Melbourne, Victoria 3010, Australia

PJG, 0000-0002-6029-515X; MP, 0000-0002-8978-7350

Advection, the *transport* of a substance by the flow of a fluid, is a key process in biological systems. The energy-based bond graph approach to modelling chemical *transformation* within reaction networks is extended to include *transport* and thus advection. The approach is illustrated using a simple model of advection via circulating flow and by a simple pharmacokinetic model of anaesthetic gas uptake. This extension provides a physically consistent framework for linking advective flows with the fluxes associated with chemical reactions within the context of physiological systems in general and the human physiome in particular.

1. Introduction

Advection is the transport of a substance by the flow of a fluid. Modelling the physiome [1–3], in particular modelling circulatory systems [4–6], requires methods for modelling the molar flows due to advection. Bond graphs have recently been used in physiome modelling due to their ability to model a wide range of biophysical systems [5]. To date, the bond graph approach to modelling biomolecular systems [7–9] considers the *transformation* of molecules via chemical reactions and the corresponding molar flow rates.

However, as pointed out by Cellier [10, p. 397] 'The term "molar flow" has … been used in two quite different contexts. On the one hand, it denotes the *physical transport* of matter from one point in space and time to another, while on the other hand, it describes the *transformation* of one chemical species into another during a chemical reaction.' In fact, both types of molar flow are needed in physiological models. For example, the binding and unbinding of oxygen dissolved in blood to haemoglobin can be viewed as a chemical reaction leading to transformation molar flow; however, the *advection* of haemoglobin though the blood stream transports the haemoglobin from the lungs to other organs and back again leading to advection molar flow. There is therefore a need to bring both transformation and advection under a common modelling framework; this paper shows how the bond graph approach can provide this framework.

Previously, *convection bonds* [11,12], which carry *two* effort variables, have been proposed, and advection has been modelled in the context of chemical reactors by Couenne *et al.* [13]. By contrast, this paper uses the standard bond graph representation with a single effort variable thus allowing standard bond graph notation and software to be used. Although energy-based modelling of distributed (PDE) systems is possible [14], this paper takes the lumped approach which is typically used for modelling the cardiovascular system [15–17] and allows the use of well-established fast ODE solvers. This paper shows how advection can be included within a bond graph model of one-dimensional fluid flow. The generation of the underlying fluid flow model is not part of this paper; general considerations such as the number of compartments to use to approximate a more detailed model of haemodynamics

taking account of flow characteristics such as the Womersley number are available [16,17]. However, the advection approach of this paper can be straightforwardly coupled to pre-existing fluid dynamics models.

Section 2 examines hydrochemical transduction—the transduction of energy between fluid flow and advected chemical potential—from a bond graph perspective. Section 3 looks at the advection of chemical species though an orifice and though a pipe and suggests a new bond graph component: **RA**. Section 4 compares and contrasts advection of chemical species via the **RA** component and transformation of chemical species via the bond graph **Re** component. Section 5 shows how circulatory advection (such as the human blood circulation) combines with binding and unbinding of a ligand and enzyme (such as haemoglobin and oxygen). Section 6 gives a numerical example of a pharmacokinetic system, representing the delivery of a gaseous anaesthetic to a human subject, based on the models developed by Mapleson [18–20]. Section 7 summarizes the paper and suggests further research.

The bond graph theory used in this paper was developed by Gawthrop and Crampin [9] and introductory material is available [21,22]. The bond graph modelling in this paper is based on the `BondGraphTools` Python package [23] available at https://pypi.org/project/BondGraphTools/. The code used for the examples in this paper is available at https://github.com/gawthrop/Advection22.

2. Hydrochemical transduction

Although different physical and chemical domains have different quantities and units, they share the same energy with units of joules (J). This fact is used by the bond graph approach to provide a unified approach to *energy transduction* between different energy domains using the transformer **TF** and gyrator **GY** elements.

This section looks at hydrochemical transduction with unidirectional incompressible hydraulic flow; bidirectional flow is considered in §3. In the incompressible hydraulic domain, the two bond graph covariables are pressure P [Pa] and volumetric flow Q [$m^3\,s^{-1}$] [24]. Noting that the unit Pa can be rewritten as $J\,m^{-3}$, the product of the covariables has units $J\,s^{-1}$. In the chemical domain, the two bond graph covariables are *chemical potential* μ [$J\,mol^{-1}$] and advective molar flow[1] f [$mol\,s^{-1}$]. The flow variables are related by

$$f_i = c_i Q_i, \tag{2.1}$$

where c_i [$mol\,m^{-3}$] is the *concentration* of the substance in the liquid.

Figure 1 shows the bond graph of a two-domain system. The section labelled *hydraulic* represents the incompressible hydraulic flow alluded to above. The **R**:$\mathbf{r_i}$ component represents an orifice though which the fluid flows; the flow Q is typically a nonlinear function of the net pressure across the orifice [5,24]. The section marked *chemical* represents a single substance being carried by the fluid though the orifice.

The hydraulic and chemical domains are connected by the transformer **TF**:$\mathbf{c_i}$ component with modulus c_i, which ensures that the chemical flow f and hydraulic flow Q are related by equation (2.1). The bond graph component

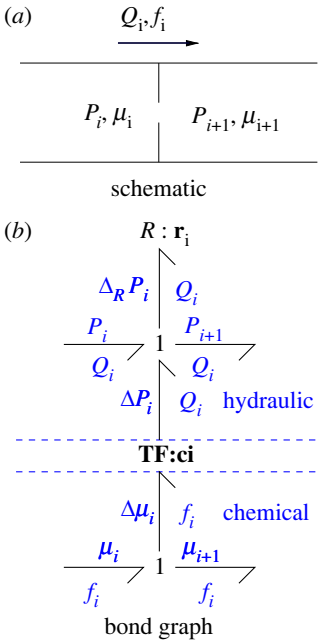

Figure 1. Hydrochemical transduction. (*a*) Hydraulic flow Q_i through an orifice with pressures P_i and P_{i+1} and chemical advection with flow f and chemical potentials μ_i and μ_{i+1}. (*b*) The bond graph **R**:$\mathbf{r_i}$ component represents the orifice hydraulic resistance, and the bond graph modulated transformer component **TF**:$\mathbf{c_i}$ transduces energy between the chemical and hydraulic domains with modulus upstream concentration c_i. The bond direction corresponds to energy flow from chemical to hydraulic and $P_{i+1} = P_i + \Delta P_i - \Delta_R P_i$ and $\mu_{i+1} = \mu_i - \Delta\mu_i$. Note that the total pressure drop $P_i - P_{i+1}$ might not be the same sign as the total chemical potential drop $\mu_i - \mu_{i+1}$ due to the pressure drop $\Delta_R P_i$ across the hydraulic **R**:$\mathbf{r_i}$ component.

transformer **TF**:**c** transmits energy, but does not dissipate energy. It follows that

$$\Delta P_i = c_i \Delta\mu_i. \tag{2.2}$$

With reference to figure 1, the energy flow, or power $\boldsymbol{P}_{TF}$, transferred by the transformer **TF**:**c** is the product of the flow and effort variables

$$\boldsymbol{P}_{\mathbf{TF}} = Q_i \Delta P_i = f_i \Delta\mu_i. \tag{2.3}$$

The power dissipated in the **R**:$\mathbf{r_i}$ component is

$$\boldsymbol{P}_R = Q_i \Delta_R P_i = Q_i(P_i - P_{i+1}) + Q_i \Delta P_i \tag{2.4}$$

$$= \boldsymbol{P}_H + \boldsymbol{P}_{TF}, \tag{2.5}$$

where

$$\boldsymbol{P}_H = Q_i\,(P_i - P_{i+1}). \tag{2.6}$$

Thus the power dissipated in the **R**:$\mathbf{r_i}$ component is the sum of the hydraulic dissipation $\boldsymbol{P}_H$ and the power $\boldsymbol{P}_{TF}$ transmitted from the chemical domain.

3. Advection

In this section, it is assumed that, although the hydraulic flow though the orifice strongly affects the chemical flow, the chemical potential has negligible effect on the hydraulic pressure across the orifice. It is therefore possible to approximate the hydraulic dynamics by neglecting the chemical dynamics and, as discussed in this section, the chemical dynamics can be reformulated in terms of a modulated resistance, thus bringing *transport* of a chemical via advection within the same conceptual framework as *transformation* via a chemical reaction.

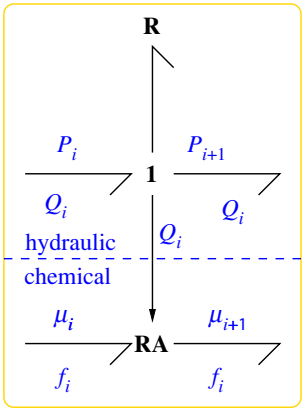

Figure 2. Advection. The transduction of figure 1 is approximated by a modulated resistive component **RA** (equation (3.2)) giving one-way interaction from the hydraulic domain to the chemical domain to represent advection of the chemical species by the fluid.

If the hydraulic flow Q_i is positive, the advective flow f_i is given by equation (2.1); if hydraulic flow Q_i is negative, the advective flow f_i is dependent on the concentration c_{i+1} rather than c_i. Moreover, the chemical potential μ_i is given in [9]

$$\mu_i = RT \ln K c_i, \tag{3.1}$$

where K is a species-dependent constant [9]. Hence the advective flow f is given by

$$f_i = \begin{cases} Q_i c_i = \frac{Q_i}{K} \exp \frac{\mu_i}{RT} \,\mathrm{mol\,s^{-1}} & \text{if } Q_i > 0 \\ Q_i c_{i+1} = \frac{Q_i}{K} \exp \frac{\mu_{i+1}}{RT} \,\mathrm{mol\,s^{-1}} & \text{if } Q_i < 0 \\ 0 & \text{if } Q_i = 0. \end{cases} \tag{3.2}$$

Equation (3.2) can be modelled as the constitutive relation of a bond graph modulated (by hydraulic flow Q_i) resistive **R** component; to reflect the special properties arising from equation (3.2) this is given a special name: the **RA** (advective **R**) component. This component is compared and contrasted with the chemical transformation **Re** component [9] in §4.

The energy flow, or power P_{RA} dissipated by the advective **R** component **RA** is the difference between the product of the flow and effort variables on the two bonds

$$P_{\mathrm{RA}} = f_i \mu_i - f_i \mu_{i+1} = f_i \Delta \mu_i. \tag{3.3}$$

From equation (2.3), it follows that $P_{\mathrm{RA}} = P_{\mathrm{TF}}$ and thus the power dissipation associated with the **RA** component in the representation of figure 2 corresponds to the power transferred by the **TF**:**c** component, and then dissipated in the **R**:$\mathbf{r_i}$ component, in the representation of §2, figure 1 and equation (2.4). Note that since the transport of chemical is driven by the hydraulic flow, P_{RA} may be negative, in contrast to a typical **Re** component which always has non-negative power dissipation.

3.1. Flow through a pipe

Although the flow of fluid though a pipe can be modelled by a PDE, it is convenient to use a lumped model instead; this has been examined in the context of blood flow by Safaei *et al.* [17]. Figure 3*a* shows a lumped model where the pipe is divided into a number of compartments, and figure 3*b* gives the corresponding bond graph. The hydraulic–chemical interaction is one-way, via the inter-compartmental hydraulic

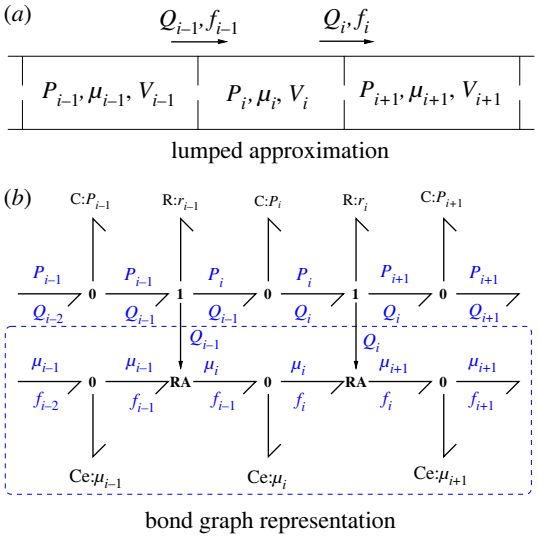

Figure 3. Flow through a pipe. (*a*) The hydraulics are approximated by a series of compartments of (possibly time-varying) volume V_i containing fluid at pressure P_i and a chemical with chemical potential μ_i. Q_i and f_i are the hydraulic and molar flow rates between compartments i and $i+1$. (*b*) The bond graph representation of the compartmental model; the advection of the chemical by the fluid is represented by the **RA** components of figure 2. If the flow rates Q_i are already determined, only the portion within the dashed box is required—this is used as the **Pipe** component in §5 and 6.

flows Q_i; thus the chemical part of figure 3*b* does not depend on the details of the hydraulic model; only the flows are required. Thus, for example, inertial terms could be added to the hydraulic model by appending bond graph **I** components to the **1** junctions [17,24].

Advection via a pipe introduces a time delay into the system dynamics, and the lumped approximation of a pipe introduces an approximate pure time delay. In particular, if the pipe has N compartments, the total pipe volume V is

$$V = \sum_{i=1}^{N} V_i. \tag{3.4}$$

In the case of identical compartments

$$V_i = \frac{V}{N}. \tag{3.5}$$

In the case of constant flow Q, the molar content $V_i c_i$ of the ith compartment has, using (3.2), a rate of change

$$V_i \frac{\mathrm{d}}{\mathrm{d}t} c_i = f_{i-1} - f_i = Q(c_{i-1} - c_i).$$

Using transfer function analysis and thus replacing $\mathrm{d}/\mathrm{d}t\, c_i$ by $s c_i$ where s is the Laplace variable, it follows that

$$c_i = \frac{1}{1 + s\tau_i} c_{i-1}, \tag{3.6}$$

where

$$\tau_i = \frac{V_i}{Q} = \frac{\tau}{N} \tag{3.7}$$

and

$$\tau = \frac{V}{Q}. \tag{3.8}$$

Hence

$$\frac{c_N}{c_0} = \left(\frac{1}{1 + s(\tau/N)} \right)^N. \tag{3.9}$$

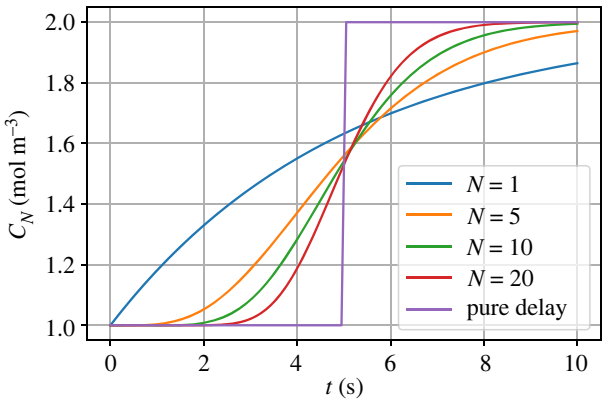

Figure 4. Dynamic response: $c_N = x_N/V_N$. With a constant hydraulic flow rate $Q = Q_0$, a step change in concentration c_0 at the downstream end of a pipe of volume $V = 5$ modelled with N compartments leads to a change in concentration c_N at the upstream end of the pipe. As N increases, the response approaches that of a pure time delay of $\tau = V/Q_0 = 5$.

Equation (3.9) is a transfer function approximation to a pure time delay $e^{-s\tau}$; in particular,

$$\lim_{N\to\infty}\left(\frac{1}{1+s(\tau/N)}\right)^N = e^{-s\tau}. \tag{3.10}$$

Figure 4 illustrates this approximation.

4. Coupled advection and transformation

As mentioned in the Introduction, there are two distinct meanings of 'molar flow': the *transport* of a substance from one place to another via advection and the *transformation* of one substance to another via a chemical reaction [10]. As discussed in §3, advection may be modelled using the **RA** bond graph component together with the capacitive **Ce** components and bonds carrying chemical potential μ and molar flow f. Moreover, transformation can be modelled by the **Re** bond graph component together with the capacitive **Ce** components and bonds carrying chemical potential μ and molar flow v [9]. Hence both concepts can be combined in a single bond graph; this combination is illustrated using a simple example. Further, it is shown how transport via the **RA** component and transformation via the **Re** component can be analysed within a common framework.

For example, figure 5*a–b* corresponds to a substance A transformed to substance C advected though an orifice with hydraulic flow Q into a well-stirred compartment within which the substance C is transformed to substance B. The substance C occurs at two locations so the corresponding **Ce** components are distinguished by denoting them **Ce:C$_1$** and **Ce:C$_2$**; the corresponding amounts of substance (C) in each location are x_1 and x_2 with corresponding concentrations c_1 and c_2.

In the case of positive flow, and in the context of figure 5*b*, equation (3.2) becomes

$$f = Qc_1 = Q\frac{x_1}{V_1}, \tag{4.1}$$

where f is the advective flow though **RA:r** and c_1 is the concentration corresponding to **Ce:C$_1$**. Figure 5*c* is identical

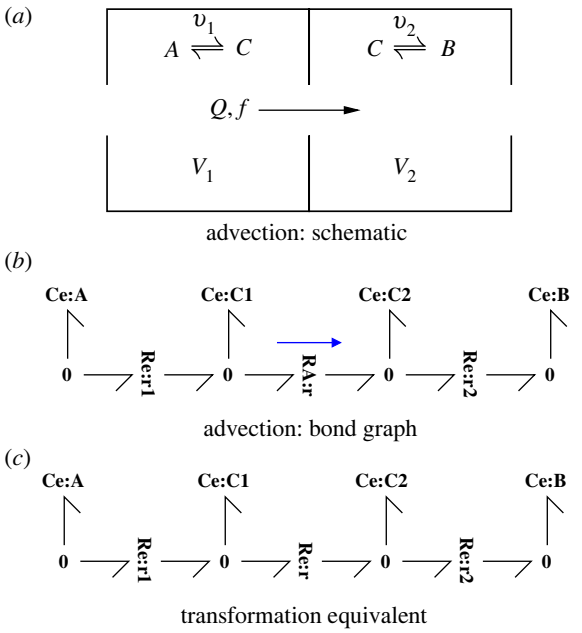

Figure 5. Coupled advection and transformation. (*a*) The schematic diagram indicates a hydraulic flow Q and advected molar flow f passing from a compartment of volume V_1 to a compartment of volume V_2. The reversible reaction $A \overset{r_1}{\rightleftharpoons} C$ occurs in the upstream compartment and the reaction $C \overset{r_2}{\rightleftharpoons} B$ occurs in the downstream compartment. (*b*) Advection is represented by the **RA** component; the unidirectional flow is emphasized by the arrow. The two reactions are represented by the **Re** components. (*c*) For the purpose of comparison, the transformation equivalent of (*b*) is shown where the **RA** component is replaced by **Re**. Figure 6 illustrates the differences between the systems of (*b*,*c*).

to figure 5*b* except that **RA:r** is replaced by **Re:r**. In this case, the transformation flow v though **Re:r** is [9, eqn. 2.2]:

$$v = \kappa_0\left(K_C^{\ominus}\frac{x_1}{V_1} - K_C^{\ominus}\frac{x_2}{V_2}\right) = \kappa_0 K_C^{\ominus}(c_1 - c_2), \tag{4.2}$$

where

$$K_C^{\ominus} = \exp\frac{\mu_C^{\ominus}}{RT} \tag{4.3}$$

κ_0 is the reaction rate-constant, and $\mu_C^{\ominus}$ is the standard potential for the species.

Equation (4.1) can be rewritten as

$$f = \kappa' K_C^{\ominus} c_1 = \kappa' \frac{K_C^{\ominus}}{V_1} x_1, \tag{4.4}$$

where

$$\kappa' = \frac{Q}{K_C^{\ominus}}. \tag{4.5}$$

In other words, the **RA** component can be modelled as a **Re** component with flow-dependent rate-constant κ' and a one-way reaction.

Equations (4.2) and (4.4) can be combined using the symbol λ where $\lambda = 0$ corresponds to equation (4.4) for advection and $\lambda = 1$ corresponds to equation (4.2) for transformation; equations (4.2) and (4.6) can be put in a common format as

$$v = \kappa\left(K_C^{\ominus}\frac{x_1}{V_1} - \lambda K_C^{\ominus}\frac{x_2}{V_2}\right) = \kappa K_C^{\ominus}(c_1 - \lambda c_2) \tag{4.6}$$

and

$$\kappa = \lambda\kappa_0 + (1-\lambda)\kappa'. \tag{4.7}$$

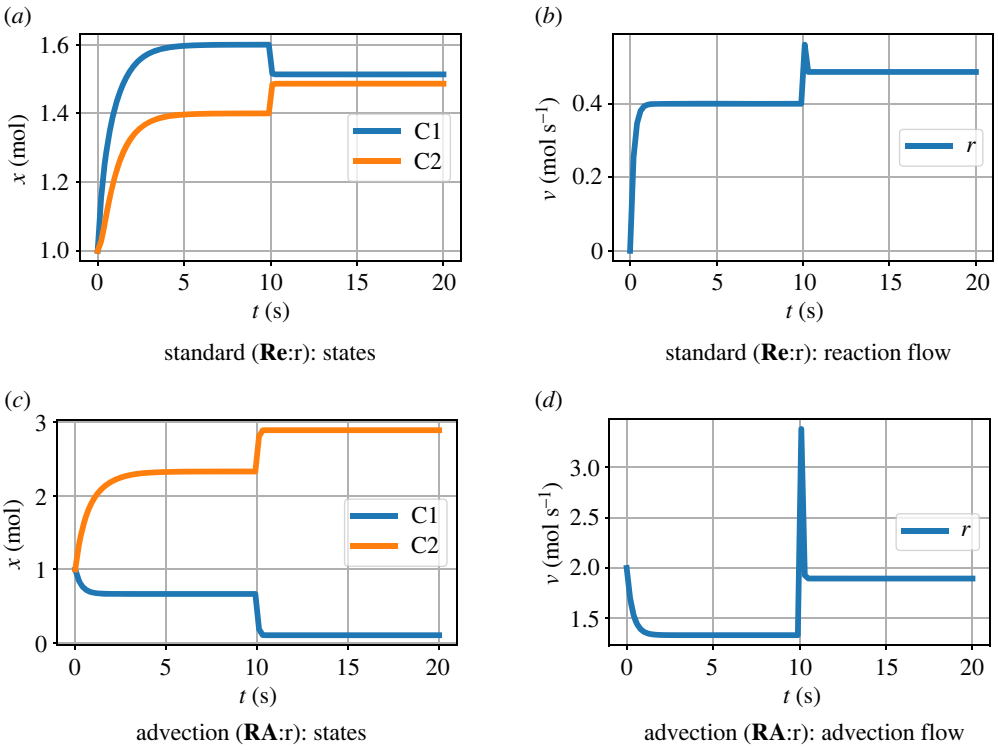

Figure 6. Coupled advection and transformation: orifice. (*a*) Amounts x_1 and x_2 when **Ce:r** is a reaction component. (*b*) The flow v_r corresponding to (*a*). (*c*) As (*a*) but when **Re:r** is an advection component. (*d*) The orifice flow corresponding to (*c*). The species components **Ce:A** and **Ce:B** fixed at constant concentations with $x_A = 2$ and $x_B = 1$; the species components **Ce:C1** and **Ce:C2** are free to vary and have unit parameters ($K_1^{\ominus} = K_2^{\ominus} = 1$). The flow $Q = 2$ when $t < 10$ and $Q = 10$ when $t \geq 10$. When $Q = 10$, the behaviour corresponds to equations (4.14) and (4.15): (*a*) $x_1 \approx x_2 \approx (x_A + x_B)/2 = 1.5$; (*c*) $x_1 \approx 0$, $x_2 \approx x_A + x_B = 3$.

Using this notation, the equations describing both figure 5*b* and 5*c* become:

$$v_1 = \kappa_1(K_A^{\ominus}c_A - K_C^{\ominus}c_1), \quad v = \kappa K_C^{\ominus}(c_1 - \lambda c_2) \quad \text{and} \quad v_2 = \kappa_2(K_C^{\ominus}c_2 - K_B^{\ominus}c_B) \tag{4.8}$$

and

$$\dot{x}_1 = v_1 - v, \quad \dot{x}_2 = v - v_2, \quad \dot{x}_1 + \dot{x}_2 = v_1 - v_2 \tag{4.9}$$

hence

$$\dot{x}_1 + \dot{x}_2 = (\kappa_1 K_A^{\ominus}c_A + \kappa_2 K_B^{\ominus}c_B) - K_C^{\ominus}(\kappa_1 c_1 + \kappa_2 c_2). \tag{4.10}$$

4.1. Illustrative example

To illustrate the difference between transportation ($\lambda = 0$) and transformation ($\lambda = 1$), consider the special case of the system of figure 5 where the rate constants of the two reactions r_1 and r_2 are the same: $\kappa_1 = \kappa_2$.

In the steady state, the time derivatives are zero and so, using equation (4.10)

$$c_1 + c_2 = \frac{K_A^{\ominus}c_A + K_B^{\ominus}c_B}{K_C^{\ominus}}. \tag{4.11}$$

If the flow Q is large, κ is also large and equation (4.8) implies that

$$c_1 \approx \lambda c_2. \tag{4.12}$$

Hence large flow in the steady state implies that

$$c_1 \approx \lambda \frac{K_A^{\ominus}c_A + K_B^{\ominus}c_B}{(1+\lambda)K_C^{\ominus}} \quad \text{and} \quad c_2 \approx \frac{K_A^{\ominus}c_A + K_B^{\ominus}c_B}{(1+\lambda)K_C^{\ominus}}. \tag{4.13}$$

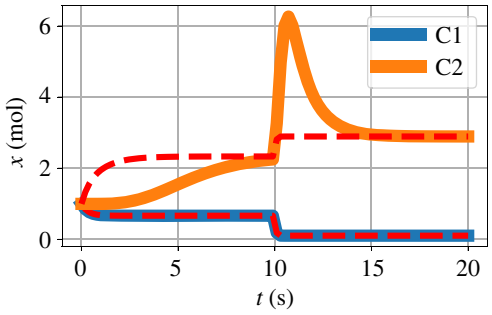

Figure 7. Coupled advection and transformation: pipe. The orifice component of figure 5*b* is replaced by the pipe model of §3.1 and the orifice results are superimposed as a red dashed line. The behaviour of x_{C1} is identical to the orifice result of figure 6*c* as the flow corresponding to the first segment of the pipe is the same as that of the orifice. Due to the pipe, the behaviour of x_{C2} is delayed with respect to the orifice case but has the same steady states.

Thus when $\lambda = 0$ (advection, figure 5*b*)

$$c_1 \approx 0 \text{ and } c_2 \approx \frac{K_A^{\ominus}c_A + K_B^{\ominus}c_B}{K_C^{\ominus}} \tag{4.14}$$

and when $\lambda = 1$ (transformation, figure 5*c*).

$$c_1 \approx c_2 \approx \frac{K_A^{\ominus}c_A + K_B^{\ominus}c_B}{2K_C^{\ominus}}. \tag{4.15}$$

The behaviour for a particular set of values is illustrated by the simulation results of figure 6. The steady-state values for large flow are explained by the analysis leading to equations (4.14) and (4.15).

Figure 7 shows simulation results corresponding to figure 6*c*,*d* but with the orifice component replaced by the pipe model of §3.1. The orifice results are superimposed as a

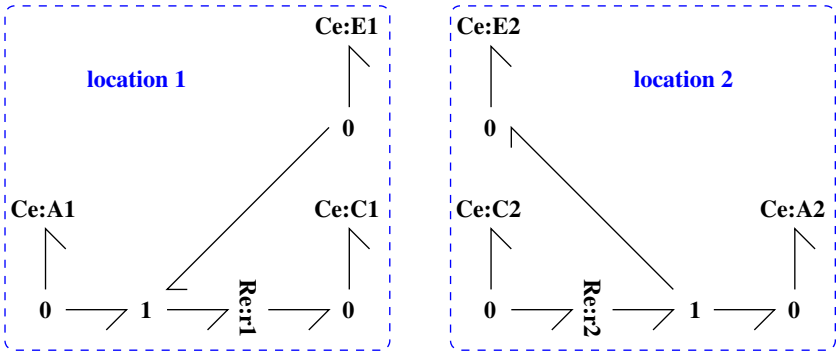

Figure 8. Split binding/unbinding cycle. At location 1, the small molecule A binds to enzyme E to form complex C; at location 2, the complex C unbinds into the small molecule A and enzyme E. C and E are transferred back and forth between the two locations by advection. For example, the small molecule A could represent oxygen and C and E could represent haemoglobin with and without bound oxygen. Location 1 could be the lungs and location 2 an oxygen-consuming organ.

dashed line and show that the steady-state values for the orifice and pipe situations are the same while the transient behaviour is different.

5. Circulatory advection

The cardiovascular systems of humans are closed in the sense that the blood is recirculated round the body: it forms a *circulatory advection* system where the blood advects many substances, notably oxygen (O_2) and carbon dioxide (CO_2). There are, in fact, a number of circulatory systems including coronary circulation, pulmonary circulation, cerebral circulation and renal circulation. The transport of O_2 involves the binding and unbinding of O_2 to haemoglobin which is itself advected by the blood.

Using a simple single circulation model, this paper shows how, in principle, the advection models of §3.1 and the advection-transformation models of §4 can be used to build models of a circulatory advection system involving binding and unbinding. More complex systems could be built using the modular properties [6] of bond graphs.

Figure 8 shows a simplified binding/unbinding cycle which has been split into two halves corresponding to two different locations. This section looks at ways in which these two halves can be connected using the advection models developed in §3. In each case, four advection connections are required to carry both bound C and unbound E enzymes to and from the two locations. Figure 9*a* shows orifice advection connections using four instances of the **RA** component of §3 whereas figure 9*b* uses four instances of the **Pipe** component of § 3.1.

If the forward and reverse orifices are identical, the two pairs of **RA** components in figure 9*a*, can be replaced by two **Re** components as shown in figure 9*c*; this is not true if the orifices are different or if pipe components are involved.

Figure 10 gives some simulation results with unit parameter values except for volume $V = 5$ and (in the case of the pipe connection) number of lumps $N = 5$.

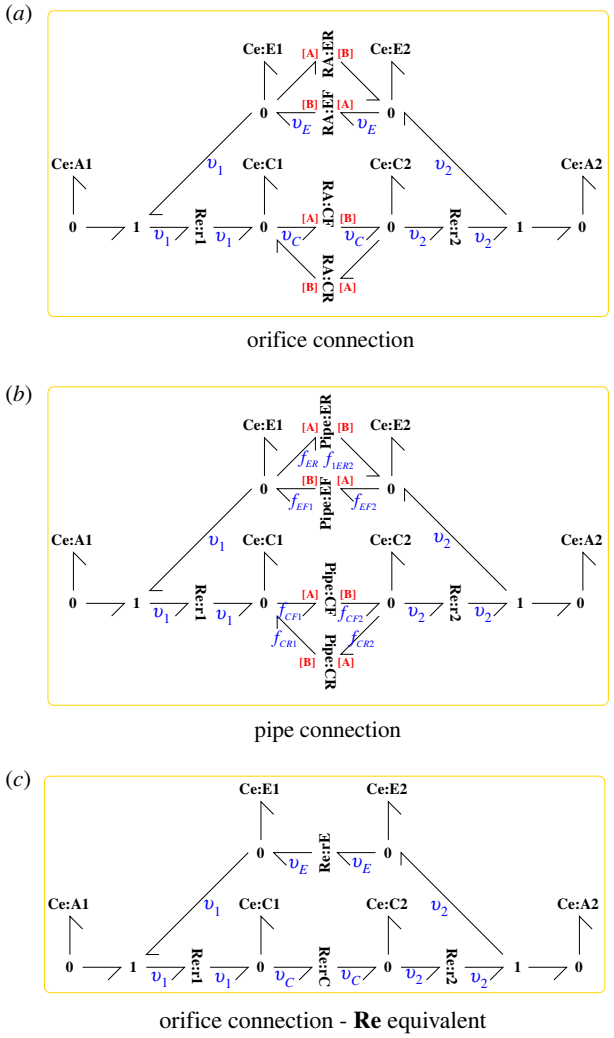

Figure 9. Circulatory advection. (*a*) Orifice advection: four instances of the **RA** component of §3 connect the two halves of the split reaction of figure 8. **RA**:**CF** corresponds to advection of the bound enzyme complex C from location 1 to 2 and **RA**:**CR** the reverse flow; **RA**:**EF** corresponds to advection of the unbound enzyme E from location 2 to 1 and **RA**:**ER** the reverse flow. (*b*) As (*a*) but using the **Pipe** component of figure 3*b*, §3.1 in place of the **RA** component. (*c*) As (*a*) but replacing the two pairs of **RA** components by **Re** equivalents.

6. Pharmacokinetics

Pharmacokinetics is the study of drug uptake in living creatures; for example, the anaesthetic gas nitrous oxide (N_2O) is administered during operations by adding it to inspired air. As it acts on the brain, the dynamics of the transfer of N_2O from the lungs to the brain via blood circulation is of interest. In his classic papers, Mapleson [18,19] gave a fully parametrized compartmental model of the uptake of the anaesthetic gas N_2O in humans outlined in figure 11. The

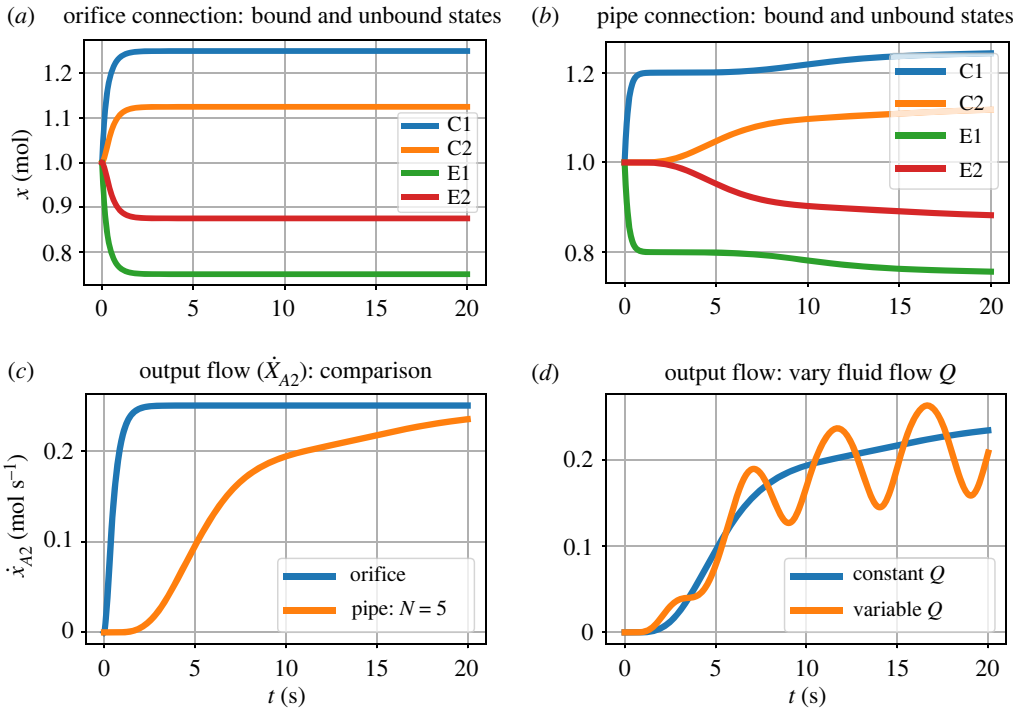

Figure 10. Simulation. For the purposes of illustration, the species *A*1 and *A*2 are held at constant concentrations with $x_{A1} = 2$ and $x_{A2} = 1$. (*a*) Orifice connection (figure 9*a*): bound (x_{C1} and x_{C2}) and unbound (x_{E1} and x_{E2}) states evolving with time *t*. (*b*) As (*a*) but with pipe connection (figure 9*b*) modelled with $N = 5$ lumps; the response is delayed with respect to (*a*). (*c*) The flow of substance A ($\dot{x}_{A2}$) into location 2 for cases (*a*) and (*b*); again, the effect of the pipe is to delay the response by about $\tau = 5$. (*d*) The output flow ($\dot{x}_{A2}$) corresponding to (*b*) but with periodically varying fluid flow $Q = 1 + 0.5\sin 2\pi t/T$ with period $T = 5$.

eight compartments are listed in figure 11; arterial blood flows from the lungs to the seven organ compartments and returns as venous blood. A simple bond graph model was given by Worship [25] and Gawthrop & Smith [26, ch. 9]. Rather than model the forking arteries and veins, following [19], the blood flow is approximated by a separate arterial flow to, and venous flow from, each compartment; the fraction δ_p of blood passing into each compartment is listed in table 1. In this section, the bond graph model of [26] is extended to explicitly include the dynamics of the veins and arteries using the approach of §3.1.

For each organ, the compartment **Ce** component has a constant K_p given by

$$K_p = \frac{1}{\lambda_p V_p}. \tag{6.1}$$

As discussed in §3.1 and with reference to table 1, the pipe parameters are

$$\kappa_p = \delta_p Q, \tag{6.2}$$

$$V_{Ai} = \frac{\delta_p V_A}{N} \tag{6.3}$$

and

$$V_{Vi} = \frac{\delta_p V_V}{N}. \tag{6.4}$$

The modular bond graph model of figure 11 was simulated and the results appear in figure 12.

The results of [19, figure 2] for the three pools (kidney, grey matter and white matter) were digitized from an image of the printed paper using the online tool https://automeris.io/WebPlotDigitizer/. As the digitized data have units of mmHg, they were normalized to be commensurate with the simulation and are shown as dots in figure 12*a*. The simulation and digitized results of figure 12*a* correspond closely; the discrepancies could be due to digitization errors, the more detailed pipe model used here, or the use of a different integration method from that used, but unspecified, by Mapleson [19].

The results shown in figure 12*b* indicate that N_2O is stored in the fat; the slow release of N_2O from the fat into the bloodstream can lead to unwanted post-operative anaesthesia [27]. In particular, at the conclusion of surgery, obese patients may wake more slowly than lean patients.

7. Conclusion

We have shown how advection can be incorporated into bond graph models of physiological systems, providing a physically consistent framework for linking advective flows with the fluxes associated with chemical reactions. This approach could be used to understand the function of a wide range of organs. Some examples include the transport of oxygen in the blood via haemoglobin; the transport of nutrients and drugs through the liver; and the transport of gases through the lungs. We believe that our approach will allow the incorporation of chemical transformation in these systems as well as transport [17,28,29]. Such models could find use in clinical contexts; for example predicting the functional consequences of surgically removing parts of the liver for cancer treatment [30] and understanding the effects of pulmonary obstruction on lung function [31,32].

Because bond graphs have already been used to model biochemical reactions [9], the models in this paper could be extended to incorporate tissue metabolism as well as advection. This has potential applications in studying the processing of nutrients by the liver and its consumption by tissue [33], as well as in understanding the metabolism

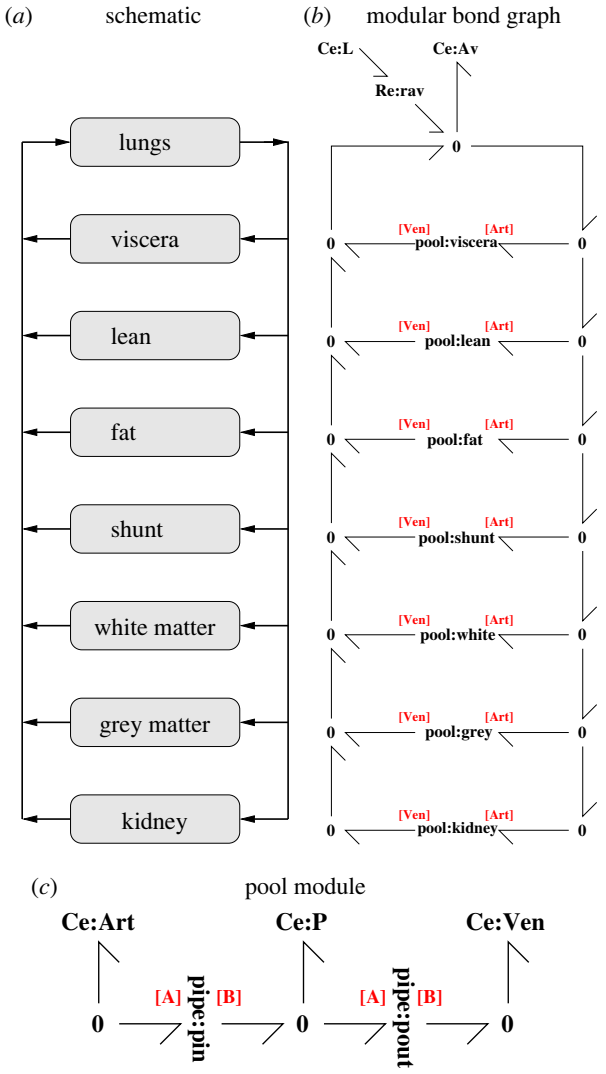

Figure 11. Pharmacokinetics: (*a*) the schematic diagram shows how the lungs are connected to six compartments representing organs together with a shunt representing blood bypassing organs [18,19]. (*b*) A modular bond graph representation of (*a*). The pool module appears in (*c*) and seven instances appear. [Art] and [Ven] correspond to the two module ports conveying arterial and venous blood respectively. The diffusion of nitrous oxide (N_2O) from the lung air (modelled by **Ce**:**L**) to the alveolar blood (modelled by **Ce**:**Av**) is modelled by the **Re**:**rav** component. The **0** junctions distribute the arterial flow and combine the venous flows. (*c*) A modular representation of a pool. The two instances of the pipe component (pin and pout) correspond to arterial flow in and venous flow out. The **Ce**:**P** component models the capacity of the pool for nitrous oxide (N_2O).

Table 1. A detailed pharmacokinetic model: data taken from tables I and II of Mapleson [19]. The volumes of arterial and venous blood are $V_A = 1.4$ l and $V_V = 4.0$ l, respectively, and the blood flow rate $Q = 6.48$ l min^{-1}. The flow fractions correspond to the 'New' column in table I of [19].

pool	vol. V_p	flow frac. δ_p	part. coeff. λ_p
lung	0.6	—	—
viscera	6.2	0.399	0.46
lean	39.2	0.364	0.46
fat	12.2	0.111	1.40
shunt	0.0	0.126	0.46
white matter	0.0007	0.000014	0.46
grey matter	0.0007	0.000055	0.46
kidney	0.0007	0.000274	0.46

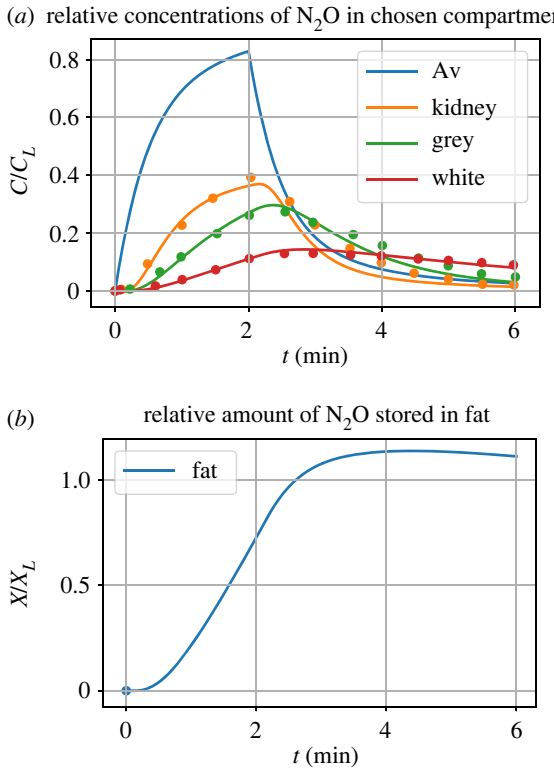

Figure 12. Simulation. Following Mapleson [19], N_2O is added to inspired air for the first 2 min; for the rest of the simulation pure air is inspired. (*a*) The concentration of N_2O, normalized by the initial concentration in the inspired air, is plotted for the alveolar blood and the kidney, brain grey matter and white matter compartments. As can be seen, the N_2O diffuses into and out of the blood via the alveoli and the concentration rises for the first 2 min and then falls as N_2O is withdrawn. Having passed though the arteries, the arterial N_2O then drives the individual compartments and is removed by the venous blood. The results of [19, figure 2] (digitized from an image of the printed paper and normalized to be commensurate with the simulation) are shown as dots. The effective time-delay of the arteries is $\tau = V_A/Q \approx 13$ s $= 0.22$ min; this delay is reflected in the initial response of the three compartmental concentrations. (*b*) N_2O accumulates in the fat and takes a long time to decay (beyond the range of this simulation).

and clearance of drugs [34,35]. The approach could also be used to model complex biochemical kinetics, for example, the cooperative binding/unbinding of oxygen to haemoglobin [36].

A benefit of the approach in this paper is that the building blocks are modular. If a finer level of detail is required, one could replace the simple models of circulation in figure 11 with more realistic models of vasculature. Furthermore, several organs have a repeating hierarchical structure that can be exploited by a modular approach. For example, the lung is composed of branching pipes that conduct the flow of gas into millions of alveoli [31]. Similarly, the liver is composed of lobes which are in turn made up of several liver lobules [30]. Once bond graph models of fundamental building blocks have been developed, they can be re-used in constructing models of more complex anatomical structures [5]. Such an approach could prove valuable for developing the multi-scale models required for the Physiome Project.

To improve the realism of the models presented here, there are some issues that require further investigation.

1. Flow typically varies across the transporting medium and thus three spacial dimensions are required for a full description of advection to include, for example, shear-induced Taylor diffusion and the effect of the Womersley number. The bond graph approach can be used to model three-dimensional fluid flow [37]; however, as discussed by Safaei *et al.* [16,17], practical full-body haemodynamic models require both one- and three-dimensional flow models; moreover, one-dimensional models can provide boundary conditions for three-dimensional models [38]. This paper focuses on modelling advection in the one-dimensional case using lumped (zero-dimensional) approximations, but future work could be directed to including advection within the three-dimensional case. The Port-Hamiltonian approach [39] provides one way forward.
2. We have assumed that the chemical domain has negligible effect on the hydraulic domain (§3). While this is in line with prior approaches [40], the validity of this assumption needs further investigation.
3. This paper considers incompressible flow through rigid pipes; in the case of blood flow the pipes are not rigid, requiring extension to compartments with variable volumes; this will be the subject of future research.
4. Hydraulic flow reversal leads to the switching function of equation (3.2). This requires further analysis, possibly using switched bond graph methods [41].
5. Species may be carried in cells within the fluid stream—for example, haemoglobin is carried by red blood cells, which may require the modelling of separate compartments.

Data accessibility. The figures and tables in this paper were generated using the Jupyter notebooks and Python code available at https://github.com/gawthrop/Advection22.

Authors' contributions. P.J.G.: conceptualization, formal analysis, methodology, software, writing—original draft; M.P.: conceptualization, formal analysis, writing—review and editing.

All authors gave final approval for publication and agreed to be held accountable for the work performed therein.

Conflict of interest declaration. We declare we have no competing interests.

Funding. This research was in part conducted and funded by the Australian Research Council Centre of Excellence in Convergent Bio-Nano Science and Technology (project no. CE140100036).

Acknowledgements. P.J.G. would like to thank the Faculty of Engineering and Information Technology, University of Melbourne, for its support via a Professorial Fellowship. M.P. is supported by a Postdoctoral Research Fellowship from the School of Mathematics and Statistics, University of Melbourne. The authors would like to thank the referees for their constructive comments which have enhanced the paper.

Endnote

[1]In this paper, the symbol v is used to represent *transformation*, and f to represent *advective*, molar flow; both have the same units: mol s^{-1}.

References

1. Diaz-Zuccarini V, Pichardo-Almarza C. 2011 On the formalization of multi-scale and multi-science processes for integrative biology. *Interface Focus* **1**, 426–437. (doi:10.1098/rsfs.2010.0038)
2. Hunter P. 2016 The virtual physiological human: the Physiome Project aims to develop reproducible, multiscale models for clinical practice. *IEEE Pulse* **7**, 36–42. (doi:10.1109/MPUL.2016.2563841)
3. Coveney P, Diaz-Zuccarini V, Hunter P, Viceconti M. 2014 *Computational biomedicine*. Oxford, UK: Oxford University Press.
4. de Bono B *et al.* 2015 The open physiology workflow: modeling processes over physiology circuitboards of interoperable tissue units. *Front. Physiol.* **6**, 24. (doi:10.3389/fphys.2015.00024)
5. de Bono B, Safaei S, Grenon P, Hunter P. 2018 Meeting the multiscale challenge: representing physiology processes over apinatomy circuits using bond graphs. *Interface Focus* **8**, 20170026. (doi:10.1098/rsfs.2017.0026)
6. Shahidi N, Pan M, Safaei S, Tran K, Crampin EJ, Nickerson DP. 2021 Hierarchical semantic composition of biosimulation models using bond graphs. *PLoS Comput. Biol.* **17**, e1008859. (doi:10.1371/journal.pcbi.1008859)
7. Oster G, Perelson A, Katchalsky A. 1971 Network thermodynamics. *Nature* **234**, 393–399. (doi:10.1038/234393a0)
8. Oster GF, Perelson AS, Katchalsky A. 1973 Network thermodynamics: dynamic modelling of biophysical systems. *Q. Rev. Biophys.* **6**, 1–134. (doi:10.1017/S0033583500000081)
9. Gawthrop PJ, Crampin EJ. 2014 Energy-based analysis of biochemical cycles using bond graphs. *Proc. R. Soc. A* **470**, 1–25. (doi:10.1098/rspa.2014.0459)
10. Cellier FE 1991 *Continuous system modelling*. New York, NY: Springer.
11. Brown FT. 1991 Convection bonds and bond graphs. *J. Franklin Inst.* **328**, 871–886. (doi:10.1016/0016-0032(91)90059-C)
12. Brown FT. 2017 Convection bond graphs for thermodynamic systems. In *Bond graphs for modelling, control and fault diagnosis of engineering systems* (ed. W Borutzky), pp. 275–309. Berlin, Germany: Springer.
13. Couenne F, Jallut C, Maschke B, Breedveld PC, Tayakout M. 2006 Bond graph modelling for chemical reactors. *Math. Comput. Modelling Dyn. Syst.* **12**, 159–174. (doi:10.1080/13873950500068823)
14. Baaiu A, Couenne F, Eberard D, Jallut C, Lefevre L, Legorrec Y, Maschke B. 2009 Port-based modelling of mass transport phenomena. *Math. Comput. Modelling Dyn. Syst.* **15**, 233–254. (doi:10.1080/13873950902808578)
15. Diaz-Zuccarini V, LeFevre J. 2007 An energetically coherent lumped parameter model of the left ventricle specially developed for educational purposes. *Comput. Biol. Med.* **37**, 774–784. (doi:10.1016/j.compbiomed.2006.07.002)
16. Safaei S *et al.* 2016 Roadmap for cardiovascular circulation model. *J. Physiol.* **594**, 6909–6928. (doi:10.1113/JP272660)
17. Safaei S, Blanco PJ, Muller LO, Hellevik LR, Hunter PJ. 2018 Bond graph model of cerebral circulation: toward clinically feasible systemic blood flow simulations. *Front. Physiol.* **9**, 148. (doi:10.3389/fphys.2018.00148)
18. Mapleson WW. 1964 Mathematical aspects of the uptake, distribution and elimination of inhaled gases and vapours. *Br. J. Anaesth.* **36**, 129. (doi:10.1093/bja/36.3.129)
19. Mapleson WW. 1973 Circulation-time models of the uptake of inhaled anaesthetics and data for quantifying them. *Br. J. Anaesth.* **45**, 319. (doi:10.1093/bja/45.4.319)
20. Hunter JM, Hemmings HC. 2019 The many contributions of WW Mapleson to the British Journal of Anaesthesia. *Br. J. Anaesth.* **122**, 159–162. (doi:10.1016/j.bja.2018.12.001)
21. Gawthrop PJ, Pan M. 2021 Network thermodynamical modeling of bioelectrical systems: a bond graph approach. *Bioelectricity* **3**, 3–13. (doi:10.1089/bioe.2020.0042)
22. Gawthrop PJ, Pan M, Crampin EJ. 2021 Modular dynamic biomolecular modelling with bond graphs: the unification of stoichiometry, thermodynamics, kinetics

and data. *J. R. Soc. Interface* **18**, 20210478. (doi:10.1098/rsif.2021.0478)

23. Cudmore P, Pan M, Gawthrop PJ, Crampin EJ. 2021 Analysing and simulating energy-based models in biology using BondGraphTools. *Eur. Phys. J. E* **44**, 148. (doi:10.1140/epje/s10189-021-00152-4)
24. Karnopp DC, Margolis DL, Rosenberg RC. 2012 *System dynamics: modeling, simulation, and control of mechatronic systems*, 5th edn. Hoboken, NJ: John Wiley & Sons.
25. Worship G. 1993 Physiological and pharmacological models for control of anaesthesia. PhD Thesis, Department of Mechanical Engineering, University of Glasgow. Supervised by P. J. Gawthrop.
26. Gawthrop PJ, Smith LPS. 1996 *Metamodelling: bond graphs and dynamic systems*. Hemel Hempstead, UK: Prentice Hall. (doi:10.5281/zenodo.6998395)
27. Hebbes CP, Thompson JP. 2018 Pharmacokinetics of anaesthetic drugs at extremes of body weight. *BJA Educ.* **18**, 364–370. (doi:10.1016/j.bjae.2018.09.001)
28. Ho H, Sorrell K, Bartlett A, Hunter P. 2013 Modeling the hepatic arterial buffer response in the liver. *Med. Eng. Phys.* **35**, 1053–1058. (doi:10.1016/j.medengphy.2012.10.008)
29. Liu CH, Niranjan SC, Clark JW, San Jr KY, Zwischenberger JB, Bidani A. 1998 Airway mechanics, gas exchange, and blood flow in a nonlinear model of the normal human lung. *J. Appl. Physiol.* **84**, 1447–1469. (doi:10.1152/jappl.1998.84.4.1447)
30. Christ B *et al.* 2017 Computational modeling in liver surgery. *Front. Physiol.* **8**, 906. (doi:10.3389/fphys.2017.00906)
31. Levy R, Hill DB, Gregory Forest M, Grotberg JB. 2014 Pulmonary fluid flow challenges for experimental and mathematical modeling. *Integr. Comp. Biol.* **54**, 985–1000. (doi:10.1093/icb/icu107)
32. Lin C-L, Tawhai MH, Hoffman EA. 2013 Multiscale image-based modeling and simulation of gas flow and particle transport in the human lungs. *WIREs Syst. Biol. Med.* **5**, 643–655. (doi:10.1002/wsbm.1234)
33. Pearson T, Wattis JAD, King JR, MacDonald IA, Mazzatti DJ. 2016 The effects of insulin resistance on individual tissues: an application of a mathematical model of metabolism in humans. *Bull. Math. Biol.* **78**, 1189–1217. (doi:10.1007/s11538-016-0181-1)
34. Reddyhoff D, Ward J, Williams D, Regan S, Webb S. 2015 Timescale analysis of a mathematical model of acetaminophen metabolism and toxicity. *J. Theor. Biol.* **386**, 132–146. (doi:10.1016/j.jtbi.2015.08.021)
35. Means SA, Ho H. 2019 A spatial-temporal model for zonal hepatotoxicity of acetaminophen. *Drug Metab. Pharmacokinet* **34**, 71–77. (doi:10.1016/j.dmpk.2018.09.266)
36. Cornish-Bowden A. 2013 *Fundamentals of enzyme kinetics*, 4th edn. London, UK: Wiley-Blackwell.
37. Baliño JL. 2017 Finite element formulation for computational fluid dynamics framed within the bond graph theory. In *Bond graphs for modelling, control and fault diagnosis of engineering systems* (ed. W Borutzky), pp. 311–358. Berlin, Germany: Springer International Publishing. (doi:10.1007/978-3-319-47434-2_9)
38. Diaz-Zuccarini V, Rafirou D, LeFevre J, Hose DR, Lawford PV. 2009 Systemic modelling and computational physiology: the application of bond graph boundary conditions for 3D cardiovascular models. *Simul. Modelling Pract. Theory* **17**, 125–136. (doi:10.1016/j.simpat.2008.04.006)
39. Argus FJ, Bradley CP, Hunter PJ. 2021 Theory and implementation of coupled Port-Hamiltonian continuum and lumped parameter models. *J. Elast.* **145**, 339–382. (doi:10.1007/s10659-021-09846-4)
40. Schwen LO, Schenk A, Kreutz C, Timmer J, Bartolomé Rodríguez MM, Kuepfer L, Preusser T. 2015 Representative sinusoids for hepatic four-scale pharmacokinetics simulations. *PLoS ONE* **10**, e0133653. (doi:10.1371/journal.pone.0133653)
41. Buisson J, Cormerais H, Richard P-Y. 2002 Analysis of the bond graph model of hybrid physical systems with ideal switches. *Proc. Inst. Mech. Eng. I* **216**, 47–63. (doi:10.1243/0959651021541426)